Fast response and low temperature sensing of acetone and ethanol using Al-doped ZnO microrods

Journal Pre-proof

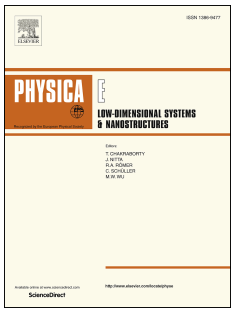

Fast response and low temperature sensing of acetone and ethanol using Al-doped ZnO microrods

Madhumita Sinha, Rajat Mahapatra, Manas Kumar Mondal, Satheesh Krishnamurthy, Ranajit Ghosh

PII: S1386-9477(19)30634-4

DOI: https://doi.org/10.1016/j.physe.2019.113868

Reference: PHYSE 113868

To appear in: *Physica E: Low-dimensional Systems and Nanostructures*

Received Date: 26 April 2019

Revised Date: 28 July 2019

Accepted Date: 4 December 2019

Please cite this article as: M. Sinha, R. Mahapatra, M.K. Mondal, S. Krishnamurthy, R. Ghosh, Fast response and low temperature sensing of acetone and ethanol using Al-doped ZnO microrods, *Physica E: Low-dimensional Systems and Nanostructures* (2020), doi: https://doi.org/10.1016/j.physe.2019.113868.

TABLE OF CONTENTS/ABSTRACT GRAPHIC:

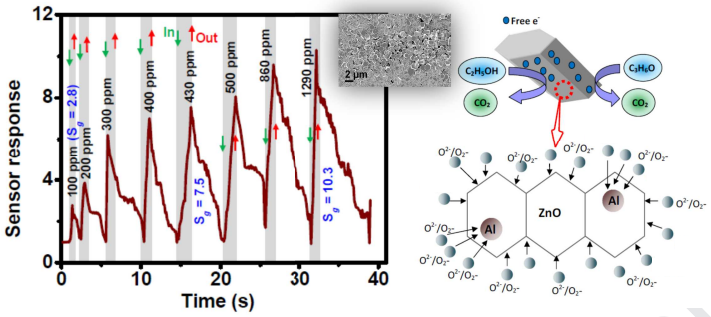

Fast response and low temperature sensing of acetone and ethanol using Al-doped ZnO microrods

Madhumita Sinha[a], Rajat Mahapatra[a], Manas Kumar Mondal[b], Satheesh Krishnamurthy[c], Ranajit Ghosh[d,e,†]

[a]*Department of Electronics and Communication Engineering, National Institute of Technology Durgapur, Durgapur 713209, India*

[b]*Department of Metallurgical and Materials Engineering, National Institute of Technology Durgapur, Durgapur 713209, India*

[c]*School of Engineering and Innovation, The Open University, Milton Keynes, MK76AA, UK*

[d]*CSIR-Central Mechanical Engineering Research Institute, Durgapur 713209, India*

[e]*Academy of Scientific and Innovative Research (AcSIR), CSIR-CMERI Campus, Durgapur 713209, India*

Abstract

We report low temperature acetone and ethanol sensing properties of Al-doped ZnO microrods synthesized using hydrothermal technique. We observe the acetone detection at room temperature as well as ethanol and acetone detection at low temperature of 150°C using Al-doped ZnO microrods. 3wt% Al-doped ZnO microrods sensor exhibits the highest response of 231 toward 8100 parts per million (ppm) of ethanol at 150°C. The response & recovery time are found to be ultrafast of 60 ms & 870 ms for ethanol and 110 ms & 330 ms for acetone of the Al-doped ZnO microrods at an operating temperature of 150°C,

† Author for correspondence, email: ghosh.ranajit@gmail.com (R. Ghosh).
Fax : +91-343-2546745

respectively. In addition, sensing mechanism has explained to illuminate the improved sensing performances of Al-doped ZnO microrods. Thus it is revealed that Al-doped ZnO microrods are promising as an ultrafast gas sensor.

Keywords: A. ZnO microrods; B. Al doping; C. Hydrothermal process; D. Gas sensor; E. Ethanol; F. Acetone.

1. Introduction

Nowadays, the presence of volatile organic compounds (VOCs) including ethanol, acetone etc. has become concern, due to its toxicity, probability of digestive track cancer and high risk respiratory symptoms. The VOCs are also known as the main cause of sick house syndrome, which is a product of poor indoor air quality and could also be the source for asthma, cancer, emphysema [1]. Ethanol, methanol, acetone, isoprene etc., which are exhaled during respiration, causes various metabolic problems. Thus, the requirement of monitoring and detection of VOCs has become progressively increased due to elevated atmospheric pollution. Acetone detection is considered as one of the important clinical analysis; can diagnose diabetes or other glucose-related dysregulation [2]. Ethanol is very useful for beverages, scientific and industrial sectors. Highly exposure and consumption of alcoholic beverages increase the risk factor of cancer. So, there is a great demand to monitor ethanol and acetone gas at trace level for health and safety [3].

Metal oxide semiconductors (MOS) devices have been one of the most promising gas sensors of which a great attention was given to zinc oxide (ZnO) for the moderate performance towards gas sensing capability [4]. ZnO is the common material for gas

sensors owing to its facile preparation process, low-cost, high chemical and physical stability. In its 1-dimensional (1D) structure its small crystal size and high density of surface active sites, makes it suitable candidate for high performance and efficiency. The sensing mechanism of the sensors depends on the changes to the resistance of the metal oxide semiconductors in the presence of the gases. The faithful mechanisms for gas response are still dubious. Usually, *n*-type semiconducting metal oxides involves the adsorption reaction to the reducing gas molecules, by releasing/trapping of electrons and thus an increase /decrease in electrical conductivity [5]. The gas response explicitly depends upon depletion region, concentrations of charge carriers, defect states and doping. Appropriate doping provides electronic defects that increase the conductivity. Few efforts have been attempted to improve mainly sensitivity properties of ZnO nanostructures by doping of Sn, Mg, Mn, Bi, Al etc. into ZnO structures [6–10]. Among them, Al-doped ZnO nanostructures are promising candidate because of its conductivity and enhanced the sensing performance. For example, Navale *et al.* [11] reported selective NO sensing characteristics of Al-doped ZnO synthesized in the form of porous pellets sintered at 350°C, and the sensor can detect small concentrations of NO at 100°C. Sahay *et al.* [12] studied the gas sensing properties of Al-doped ZnO thin films prepared by chemical spray pyrolysis technique. It was observed that Al-doped films show higher sensitivity to ethanol vapor compared to the undoped ZnO film. Li *et al.* [13] reported the synthesis of Al-doped ZnO nanotetrapods by thermal evaporation of the mixed powders of Zn and Al with the weight ratio of 5:1, and the ethanol sensing properties are effectively improved by Al doping. Badadhe *et al.* [14] developed Al-doped ZnO thin films on to the glass substrates and discussed the gas sensing to H_2S gas.

Generally, ZnO nanostructures was synthesized by different growth techniques such as physical vapor deposition, metal–organic chemical vapor deposition (MOCVD), pulsed laser deposition, molecular beam epitaxy (MBE), electro-spinning, sputtering, wet chemical methods etc [15–18]. Among them, wet chemical methods are striking for several reasons due to its low cost, easy scaling up and growth occurs at a comparatively low temperature [19]. In addition, the development of a highly responsive and selective ZnO-based sensor is significant for the detection of VOCs at low temperature and low concentration also. One of the major challenge in the development of high performance gas sensors is that it can function at low temperature even at room temperature (RT) having low power consumption, sensor's good stability and longer lifetime. Furthermore, sensor at RT can be operated at many undesirable situations (flammable or explosive environment) [20,21].

We report low cost and low temperature (~95°C) synthesis of aligned Al-doped ZnO microrods by hydrothermal technique and enhancement of gas sensing performance towards acetone and ethanol at RT as well as 150°C. In addition, it is aimed to augment the sensing parameters such as fast response time and high sensitivity gas sensor obtained by Al-doping in ZnO.

2. Experimental details

2.1 Synthesis of Al-doped ZnO microrods

All chemical reagents were used in this experiment is of analytical grade. The Al-doped ZnO microrods were grown by hydrothermal technique and the details were described in our previous reports [22]. In brief, a clean glass substrate was coated with 4-layer ZnO thin film by sol-gel technique. ZnO thin film was prepared using the solution of zinc acetate dehydrate [$Zn(CH_3COO)_2 \cdot 2H_2O$], diethanolamine [$HN(CH_2CH_2OH)_2$] and

isopropyl alcohol [$CH_3CHOHCH_3$]. A dip coater was used for coating the glass substrate and after every coating the films was annealed at 120°C in hot oven for 1 h followed by annealed at 350°C for 1 h. This process was continued for successive 4 times. In the next step, a mixture of equimolar (50 mM) aqueous solution of zinc acetate dehydrate [$Zn(CH_3COO)_2 \cdot 2H_2O$], hexamethylenetetramine [$(CH_2)_6N_4$] and aluminium nitrate nonahydrate [$Al(NO_3)_3 \cdot 9H_2O$] were prepared after thoroughly mixing in di-ionized water (Milli Q, Resistivity >18.2 MΩ·cm) on a magnetic stirrer at room temperature. Finally, microrods were synthesized by dipping 4-coated ZnO thin films in the solution at 95°C for 1 h. The substrate was removed from the solution, rinsed with ultrapure water and air dried for further characterizations. The Al^{3+} concentration was varied from 1–4wt% to evaluate the effect of Al doping in ZnO toward VOCs sensing performance with respect to undoped ZnO.

2.2 Characterizations of Al-doped ZnO microrods

The crystallinity and orientation of the samples were examined by X-ray diffractometer (XRD) (X' Pert PRO, PAN analytical) using a CuKα1 radiation (1.5406 Å). A range (30-70°) of scanning was performed for scanning angles 2θ. The surface morphology of Al-doped ZnO structures were investigated by using a field emission electron microscope (FESEM) (evo 60, Carl Zeiss) equipped with an energy-dispersive X-ray (EDX) spectrophometer. Surface characterization was carried out using atomic force microscopy (AFM) (Nanosurf, C3000). Electronic properties and surface characteristics were investigated. X-ray photoelectron spectroscopy (XPS) (Kratos, XSAM 800) was carried out with non-monochromatic Mg (hv =1253.6 eV) radiation. All binding energies were calibrated by referencing to the C1s peak at 284.6 eV. The gas sensing measurements

were carried out using a lab made sensing set-up. The schematic structure of the sensing element is shown in Fig. 1(a). Two copper probes in lateral position on the top of surface were used to make the electrical contacts with the sensing elements. Fig. 1(b) shows the photograph of the sensor element with two cupper probes connection, which is placed on the heater equipped with proportional-integral-derivative temperature controller (DCS-PWR-2K5-10AC-024, Dynamic Control System). The current of the sensor was recorded using a source-measure electrometer unit (6517A, Keithley Instruments). The transient current was measured at a 5 V bias and with a time interval of 1 ms in this experiment. For *n*-type semiconductor, the relative response (S_g) of the gas sensor is defined as **Equation 1:**

$$S_g = G_g/G_a \quad (1)$$

where G_g is the conductance measured in the presence of the VOCs (acetone and ethanol) being detected and G_a is the conductance in air (i.e., in the absence of the VOCs being tested). A known amount of VOCs was injected into the gas chamber and subsequently, the increase in conductance was monitored till in the closed condition. Finally, one end of tube was opened and air was pumped to about 10^{-2} mbar to recover the initial value of conductance in air. The sensing measurements were carried out at RT as well as at 150°C under different concentration (25 to 8100 ppm) of VOCs (acetone and ethanol) vapor. Acetone ($(CH_3)_2CO$, d_v = 0.79 g/cm^3, M_w = 58.1 g/mol) 0.6–188 μL [about 25–8100 parts per million (ppm)] and ethanol (CH_3CH_2OH, d_v = 0.79 g/cm^3, M_w = 46.07 g/mol) 0.5–150 μL (about 25–8100 ppm) were used as a liquid and the liquid was injected into the gas chamber through a micro-syringe with a volume precision of <2.5%. The experiment was done in presence of a relative humidity of 26%.

The concentration in ppm could be calculated according to **Equation 2 [**23]

$$C(\text{ppm}) = \left(\frac{d_v V_{injected}}{M_w V_{chamber}}\right)\left(22.4\,\frac{\text{L}}{\text{mol}}\right)10^6 \quad (2)$$

where C(ppm) is concentration of VOCs in ppm, d_v is the liquid mass density (g/cm^3), $V_{injected}$ is the injected volume in μL, M_w is the molar mass of the liquid (g/mol), $V_{chamber}$ is the volume of chamber of 7 L.

3. Results and Discussion

3.1 Structural studies

The phase composition and crystallinity of the as synthesized undoped and Al-doped ZnO samples were investigated by XRD. XRD patterns of undoped ZnO (JCPDS Reference no. 80-0075) and Al-doped ZnO (1–4wt%) are shown in Fig. 2. All the peaks are indexed mainly to wurtzite hexagonal shaped ZnO [Joint Committee on Powder Diffraction Standards (JCPDS) Reference no. 80-0075]. XRD analysis reveals that all Al-doped materials have preferred (002) orientation, confirming *c*-axis growth. This is due to the lowest surface energy of the densely packed (002) planes of the wurtzite structure [24]. No other phases corresponding to aluminium or aluminium compound is detected in XRD patterns till 3wt% Al doping in ZnO. This may indicate that the precursors have fully been converted into ZnO phase, and Al doping does not alter the hexagonal structure of the ZnO lattice. For 4wt% of Al doping, Al_2O_3 phase separation has been occurred, as shown in Fig. 2. This is because beyond a certain doping limit (3wt% Al for this report), the doping atoms may result in some kind of segregation in crystal. However, with increasing Al doping concentration, the diffraction angles do not change significantly and only the dominant (002) peak becomes sharper, indicating the well-established *c*-axis orientation of Al-doped ZnO. Although, a marginal shift of the peaks ((100), (002) and (101)) of chemically prepared ZnO nanoparticles doped with Gd, Er and Li was reported by Li *et al*. [25].

The preferred orientation of the crystals planes was obtained by measuring the diffraction peak intensities corresponding to the various planes of XRD. The texture coefficient (T_c) of corresponding to diffraction plane (*hkl*) is calculated in **Equation 3** utilizing the following equation [26]

$$T_c(hkl) = \frac{I_{o(hkl)} / I_{std(hkl)}}{(1/N)\sum I_{o(hkl)} / I_{std(hkl)}} \quad (3)$$

where, $I_{o(hkl)}$ is the observed intensity of X-ray diffraction, $I_{std(hkl)}$ is the corresponding standard intensity from the JCPDS data (card No. 80-0075) and *N* is the number of reflections in the XRD pattern. The T_c values for the first three characteristics peaks (100), (002), (101) are calculated and presented in **Table S1** (see supporting information). The texture co-efficient against (002) peak is 0.47 for undoped ZnO and 0.9 for 1wt% Al-doped ZnO microrods. The similar texture coefficient of 0.5 was also reported elsewhere for ZnO films [27]. All Al-doped ZnO nanorods exhibit enhanced intensities relating to (002) peak with respect to (100) and (101) peaks, which show a preferential orientation along c-axis. The high crystallinity, together with very good texture coefficient may enhance the result of gas sensing.

The lattice parameter *c* of hexagonal wurtzite crystal structures of all the samples are calculated by using the following equation [28]

$$d_{(hkl)} = \sqrt{\left[\frac{4}{3}\left(\frac{h^2+k^2+hk}{a^2}\right) + \frac{l^2}{c^2}\right]} \quad (4)$$

For (002) peak **Equation 4** becomes

$$d_{(002)} = \frac{4}{c^2} \quad (5)$$

The calculated values of *c* are listed in **Table S1**. There is hardly change of lattice parameter (*c*) with increase in Al concentration on ZnO. This is due to comparable ionic radius of Al^{3+} (0.53 Å) to the ionic radius of Zn^{2+} (0.60 Å). Mridha *et al.* [29] reported the similar results that the *c*-axis length does not change much with the various Al concentrations (0.5 – 5%) for ZnO: Al nanoparticles thin films deposited on glass substrate by the sol–gel spin coating technique.

3.2 Morphological study and chemical analysis

Fig. 1(c) shows the typical SEM image of 3wt% Al-doped ZnO microrods. All the hexagonal microrods of diameter in the range of 400-900 nm are vertically oriented to the substrate surface. This oriented growth indicates that ZnO microrods are grown along *c*-axis, which is also confirmed by XRD (Fig. 2). The lengths of grown microrods are 2–5 μm. There is no significant change of structures of hexagonal microrods for different percentage of Al-doped ZnO. Furthermore, morphology of the Al-doped ZnO microrods was also examined by AFM, as shown in Fig. 3. It can be inferred from Fig. 3(a)-(d) that ZnO microrods are oriented with an average diameter of 800 nm. There is no separate phase of Al_2O_3 for 1-3wt% Al-doped ZnO samples (Fig. 3(a)-(c)). However, a large number of white particle-like structures of Al_2O_3 on the surface of ZnO microrods is prominent for 4wt.% Al-doped ZnO sample (Fig. 3d). The separate phase of Al_2O_3 for 4wt% Al-doped ZnO microrods was also confirmed by XRD.

Elemental analysis of 3wt% Al-doped ZnO micrords was conducted by EDX, as shown in Fig. S1 (see, supporting information). The results confirm the existence of Zn, O, Al elements in the Al-doped ZnO micrords. No impurities were found in the sample.

XPS studies were carried out to understand the electronic properties, surface and chemical composition of the elements of the samples. Fig. 4 shows the high-resolution XPS spectra of Zn 2p, O 1s, and Al 2p of undoped ZnO and 3wt% Al-doped ZnO samples. Zn 2p core level spectra present the typical doublet splitting of Zn $2p_{3/2}$ and Zn $2p_{1/2}$, as shown in Fig. 4(a). The intense peak at 1021 eV corresponds to Zn $2p_{3/2}$ and the other one at 1043.8 eV corresponds to Zn $2p_{1/2}$, which are well matched with the standard values of ZnO [30]. However, changes are observable at the O 1s core level spectra. With doping the line width of the peak has increased. This may be due to increase in concentration of hydroxyl groups or due to increase in concentration of chemically absorbed oxygen species on the surface with Al doping. O 1s spectra show different states of oxygen existence in the samples. The component with the lowest binding energy, centered at 530.15 eV, is attributed to O^{2-} ions on wurtzite structure of hexagonal Zn 2p array surrounded by the substitution of Al atoms (Fig. 4(b)). The other peak at 532.3 eV for Al doped ZnO sample (Red dotted curve) is attributed to chemisorbed oxygen ions (O^{2-} or O^{-}) on the surface of ZnO [31]. XPS analysis clearly indicates that the sample of 3wt% Al-doped ZnO contains more defects on the surface which will enhance the gas sensing property. The successful incorporation of Al elements in Zn^{2+} sites of ZnO is confirmed from the clear peak of Al 2p at the binding energy of 74.1 eV and it is in Al^{3+} state as shown in Fig. 4(c). In comparison, the intensity is very tiny for Al 2p peak than that of Zn $2p_{3/2}$ peak because of the dilute aluminium concentration in the specimens. There is no peak observation of Al for undoped ZnO sample.

3.3 Gas sensing performances

The sensing properties of the Al-doped ZnO microrods toward ethanol vapor detection at a low temperature of 150°C were initially investigated using different wt% of Al doping in ZnO. Fig. 5 shows the variations of response with different percentage of Al doping in ZnO towards 500 ppm ethanol at an operating temperature of 150°C. It should be noted that the response values were estimated using the **Equation 1** for taking into account of the average values of three successive measurements. For all Al-doped ZnO microrods, the response increases with increase with Al doping and 3wt% Al-doped ZnO microrods shows maximum response (G_g/G_a) of 15, which is about 7 times higher than that of undoped one. After that response of the senor drops to 3.8 for 4wt% Al doping in ZnO. A set of factors that control the enhancement of sensing performance, including surface facet, surface oxygen defects and the conductivity of the materials, are considered [32]. However, it is well established that the conductivities of Al-doped ZnO materials are higher than that of pure ZnO because of the Al^{3+} ions (as confirmed from XPS), which introduces extra electrons into the doped ZnO [33]. The decrease in resistance due to Al doping in ZnO sample may be occurred via the charge compensation mechanism:

$$Al_2O_3 + ZnO \rightarrow Zn_{Zn} + 2Al_{Zn} + 3O_{Ox} + (1/2)O_{2(g)} + 2e^- \quad (6)$$

Previous report [29] showed a maximum conductance occurs at intermediate Al doping (i.e 1wt%), after which the conductance decreases. Moreover, 3wt% Al-doped ZnO microrods show higher texture co-efficient of 0.24 along (101) crystal facet supported by Fig. 2 & **Table S1**. As, (101) crystal facet of ZnO is thermodynamically favorable for the absorption of ethanol, 3wt% Al-doped ZnO microrods show the highest response. Therefore, 3wt% Al doped ZnO microrods has used further to confirm the gas sensing performances.

The typical dynamic response behavior toward ethanol of various concentrations at a temperature of 150°C for 3wt% Al-doped ZnO is investigated and shown in Fig. 6. The response is 7.3 for low concentration (25 ppm) of ethanol. Interestingly, the base conductance in air i.e, without ethanol vapor is $1.16\times10^{-8}\ \Omega^{-1}$ and increases to 9.6×10-8 Ω^{-1} in presence of 25 ppm of ethanol vapor. Finally, it is reversed back to 9.4×10-9 Ω^{-1} when air is introduced again. Therefore, the developed Al-doped ZnO microrods based sensor is a purely reversible-type, which is one of the most basic requirement of a sensing element for its device adaptability, since switched forth and back of conduction between the test vapor (during response process) and air (during recovery process) [34]. Further, the response increases with increase in ethanol vapor concentrations. The highest response is found to be 231 toward 8100 ppm of ethanol vapor. **Table 1** shows the comparison of ethanol sensing properties of reported doped sensor and the developed gas sensor in this work. For example, Lee *et al.* prepared Ga (3wt%) doped ZnO nanowires using plasma laser deposition in a furnace and reported the response of 48% using 1ppm of ethanol vapor at an operating temperature of 300°C [35]. Yang *et al.* was synthesized Al (2wt%) doped ZnO microstructure and reported 3000 ppm ethanol detection to get 200 responses at a high operating temperature of 290°C [36]. Sayed *et al.* showed the response values of 85 and 120 using nanoparticles of ZnO with 4wt% CeO_2 and SnO_2 with 2wt% CeO_2 mixed samples where 100 ppm ethanol gas were used at 400°C for their study [37]. Above all these reports are ethanol sensing but shows comparatively in higher operating temperature. Therefore, the result of ethanol sensing in this work shows higher response at low operating temperature compared to other reported results.

The comparison of response toward different concentrations (25–8100 ppm) of ethanol for 3wt% Al-doped ZnO microrod sensor has been studied with another VOC i.e acetone at the same operating temperature of 150°C. Fig. 7 shows the variation of the response with ethanol and acetone vapor concentrations (25–8100 ppm). At lower concentrations (inset of Fig. 7), there is a linear relationship between response and vapor concentration for the tested VOCs (ethanol and acetone), which is the conformity with the theory of semiconductor based sensors [38,39]. However, the saturation response occurs at higher concentration (above 600 ppm) due to the saturation of surface coverage. It is observed that the Al-doped ZnO microrods sensor clearly exhibits the highest response (S_g) of 231 at 150°C toward 8100 ppm of volatile ethanol vapor. This is the highest the response toward acetone, indicating the excellent selectivity of the Al-doped ZnO microrods sensor toward 8100 ppm volatile ethanol gas at 150°C. The result indicates that Al-doped ZnO microrods sensor would have great potential for detecting ethanol at high concentration but comparatively low temperature of 150°C for semiconductor sensor.

However, the ultimate goal in the sensor technology is to detect VOC at room temperature. To examine the potential of Al-doped ZnO microrods sensor operating at room temperature, the gas sensing properties of 3wt% Al-doped ZnO microrods using different concentration of acetone at RT have been investigated. Interestingly, it shows a moderate response toward acetone even at room temperature. There is a negligible response using ZnO based microrod sensor toward ethanol at room temperature. This phenomenon has explained later. To investigate the transient characteristics of 3wt% Al-doped ZnO microrods, the sensor is exposed to different acetone concentration at room temperature, as shown in Fig. 8. Even below 100 ppm, it was hard to measure the response behavior of the

materials at room temperature. However, the highest response of 10.3 is obtained for 1290 ppm acetone. An appropriate amount of a metal has been shown to have higher catalytic activity and lead to the consumption of a large amount of oxygen adsorbates at lower temperature. As electron donors, acetone molecules need to be dissociated into more active atoms [40].

The reliability of the sensors is another important parameter along with high response and selectivity. The repeat sensing measurement was conducted after 6 months using the same 3wt% Al-doped ZnO microrod sample at room temperature in presence of different concentration of acetone vapor to confirm the reproducibility and long-term stability of the samples and it is depicted in Fig. 9. It has been noticed that the ZnO sensor exhibits excellent stability toward acetone with the response amplitude values 2.8 and 11.6 for 100 ppm and 1290 ppm, respectively, toward acetone at room temperature.

The observed sensor parameters for acetone sensing at room temperature is compared to previously reported sensor materials, as shown in **Table 2**. It is observed that the our as-grown Al-doped ZnO microrods sensor is high sensitive to acetone at room temperature as compared to reported elsewhere. For example, Zhang *et al.* demonstrated room temperature acetone gas sensor based on SnO_2–reduced grapheme oxide (RGO) hybrid composite film with the response [$S_g(\%) = (R_a - R_g)/R_g \times 100$] 2.19-9.72% at 10-2000 ppm gas and the response-recovery time was 146 s – 141 s toward 2000 ppm of acetone [41]. Do *et al.* reported response of $1.19\text{-}4.03\times10^{-7}$ for 2983-47925 ppm acetone at room temperature for PPy-PANI [42]. Behera and Chandra presented a simple and cost-effective MEMS sensor incorporating ZnO–CuO nanoflakes [43]. The fabricated sensor showed an optimal response (12.6) at 300°C with improved selectivity to acetone. On the

other hand, Yoo *et al.* prepared Al-doped (1wt%) ZnO nanoparticle, in which the response was 4347 at 350°C temperature using 10 ppm dimethylphosphonate [44]. Hence, it is clear that our developed 3wt% Al-doped ZnO microrod sensor is superior response to acetone at low temperature.

The response and recovery times are another important parameters of gas sensor, have been calculated from the typical response plots of Al-doped ZnO microrods gas sensor. The response time is defined as the time it takes for conductance/resistance of the gas sensor to increase to 90% of the conductance/resistance change when a specific amount vapor was introduced into the sensor test chamber. The recovery time is the time required for a 90% reduction in conductance/resistance change when the gas was turned off and air was re-introduced into the chamber.

The response and recovery time of the gas sensor towards acetone and ethanol vapor with different gas concentration at RT as well as at 150°C are shown in Fig.10. For 100 ppm acetone at room temperature (Fig. 10(a)), the response and recovery time are 430 ms and 960 ms, respectively, which is ultrafast detection time and useful in practical application as a sensor. It is noted that semiconductor based gas sensor generally showed the long response and recovery time in second (s) region. The response time (Fig. 10(b)) varies from 110 ms to 510 ms to reach 90% of its response in presence of acetone vapor and the recovery time (Fig. 10(c)) varies from 960 ms to 15.4 s due to 90% reduction of response when air was turned on of Al-doped ZnO microrods sensor at room temperature. At 150° C the response time varies between 110 ms to 2.11 s and the recovery time is between 330 ms to 34.9 s from 25 ppm to 6450 ppm acetone vapor. The response time is nearly same for both the RT and at 150°C while recovery time has increased with the

concentration of acetone vapor. It clearly indicates that the response time is very fast in comparison to the recovery time. In the case of ethanol, the response times are increased from 60 ms to 700 ms with the increase in concentration. Similarly, the recovery times are also gradually increased from 870 ms to 11.13 s.

From **Table 1** and **Table 2**, it is easily found that the very fast response time is observed in the present work. Using dimethylphosphonate the measured response time was 2 s to few minutes for ZnO materials [44,45]. For Al-doped ZnO nanomaterials, response time and recovery time of 8 s and 10 s were calculated by Yang *et al.* [36]. Comparatively faster response and recovery time of 1 s and 5 s respectively was reported by Zhang *et al.* for Sn doped ZnO nanostructures, where gas sensing measurement was carried out in presence of ethanol gas and irradiation of light [46]. The response time and recovery time was obtained 12 s and 10 s respectively by Sayed *et al.* [37].

3.4 Gas sensing mechanism

Initially, when ZnO microrods are placed in ambient condition, the O_2 molecules adsorb on the ZnO microrod surface trapping the free electrons and the formation of ionized (O_2^-, O^- or O^{2-}) species [47,48]. The ionized oxygen (O_2^-, O^- or O^{2-}) species extracts electrons at different temperature from the conduction band and an electron depletion region is formed, which increases the resistance of individual microrod [47,48]. This exchange will contribute to the decrease of the net carrier density in the microrods conductance channel. For a high-purity ZnO microrods, the charge carrier concentration decreases. Thus, the position of the Fermi level shifts away from the band gap throughout the entire microrods and electrons move independently [49]. On the other hand, for metal semiconductors, doping is a good approach to modulate the thickness of the depletion

region and get enhanced response from ZnO nanostructures [50]. Thus, it is possible to control sensitivity, selectivity, and response time of doped micro-structures. When ZnO is doped with Al, the dopants may act as singly charged donors and these supply the excess carriers to conduction band, which increases the conductivity. Dopant Al in ZnO amplifies the electrical conductivity due to the substitution of Zn^{2+} by Al^{3+}, since there is large ionic difference between Al^{3+} ions (0.054 nm) compared to that of Zn^{2+} (0.074 nm) [12]. There are a number of donor defects in the ZnO crystal structure. The electron is produced by the defects of O or Zn in ZnO without Al, while after Al doping, an extra electron and an oxygen vacancy are generated. As a result, the amount of the current carrier is enhanced. When ZnO microrods are exposed to ambient condition, their surfaces would be adsorbed by O^{2-}/O^{-} species having E_{ads} = -0.35 eV/mol at low temperature below 200 °C. The adsorbed oxygen species captures electrons from conduction band and hence the samples will be forced back to the semiconducting configuration. While, ethanol or acetone is introduced in the test chamber leading to increase in conductivity. This may be effected by two subsequent phenomena occurring at the microrods surface: (i) since ethanol and acetone has a higher adsorption energy (E_{ads} = -0.96 eV/mol for ethanol and E_{ads} = -0.8 eV/mol for acetone) compared to adsorbed oxygen species (E_{ads} = -0.35 eV/mol), it is able to remove oxygen from the surface, (ii) this is accompanied by freeing trapped electrons which are injected back to the conduction band (CB), leading to enhanced surface conductivity. Therefore, surface carrier charge density will closely be linked to the concentration of ethanol or acetone in the atmosphere and higher conductivities should be attained when O_2 molecules are completely removed from the surface. The sensing mechanism is depicted in Fig. S2 (see, supporting information). Al-doped ZnO microrods

are adsorbed more ionized oxygen which exposed to the ethanol and acetone at 150°C. These additional adsorbed oxygen molecules on the surface of microrods will be reacted with ethanol or acetone molecules as the following reactions, presented **Equations 9** and **10,** respectively. Ethanol and acetone is oxidized into carbon dioxide and leave the sensor surface during recovery [51,52].

$$O_2\ (gas) \leftrightarrow O_2\ (adsorbed) \quad (7)$$

$$O_2\ (adsorbed) + e^- \leftrightarrow O^{2-}/2O^- \quad (8)$$

$$C_2H_5OH + 3O^{2-} \rightarrow 2CO_2 + 3H_2O + 6e^- \quad (9)$$

$$C_3H_6O + 4O^{2-} \rightarrow 3CO_2 + 3H_2O + 8e^- \quad (10)$$

Al has observed to be an effective catalyst in detection of VOCs by enhancing the rate of chemical sensitization [53,54], which greatly affects the dissociation of oxygen molecules and increases the ionosorption of the dissociated oxygen species on the surface of the ZnO microrods. As an effect of this, the electron depletion region becomes wider. When the Al-doped ZnO microrods are exposed to VOCs, it causes the electrons trapped by the dissociated oxygen species and it is injected back into the conduction band of the metal oxide. As a consequence, the decrease of the electrical resistance and an enhanced sensor response can be occurred. Therefore, it is reasonable to accept the fact that with the catalytic metals, the gas sensing performance is enhanced at 150°C.

Furthermore, Al-doped ZnO shows a significant performance toward acetone sensing, while no sensing performance observed for ethanol at room temperature. Generally, the polarity of VOC and stoichiometry of the crystal faces a play role for high sensitivity performances at room temperature, since dissociation steps in the above mentioned mechanism (**Equation 8**) has to be occurred only at high temperature like

150°C [54]. Therefore, oxidation of the VOC molecules occurs at room temperature due to pre-absorbed oxygen specie O^{2-}, which is less chemically active. Generally, the adsorption energy for acetone (-0.8 eV/mol) on the surface is smaller in magnitude than ethanol (-0.96 eV/mol), but higher than oxygen (-0.35 eV/mol), a weaker binding energy for acetone on the surface [32]. This is due to the higher polarity of ethanol vapor compared to acetone. As, the polar hydroxyl group $(O\text{-}H)_{EtOH}$ of ethanol interacts with sensor surface via two binding modes (Al 2p-O_{EtOH}) and ($O_{lattice}$-H_{EtOH}), while carbonyl group (C=O) of acetone directly interacts with the surface Al cations, which is favourable to the good sensing properties of acetone at room temperature.

4. Conclusions

A study on the hydrothermally grown Al-doped (1-4%) ZnO microrods have been carried out for detection of VOCs like ethanol and acetone. XRD study reveal that all the materials are possessing hexagonal wurtzite structure with a preferred (002) orientation. Al-doped films are highly sensitive to acetone and ethanol compared to the undoped ZnO microrods. Among all the Al-doped samples, the 3wt% Al-doped ZnO microrods exhibits the maximum response of 231 toward 8100 ppm of ethanol at an operating temperature of 150°C. On the other hand, the response is found to be 2 for undoped ZnO film toward 500 ppm concentration of ethanol at the temperature of 150°C. Furthermore, the 3wt% Al-doped ZnO microrods sensor shows higher response toward acetone compared to ethanol in low concentration region of 200-500 ppm at 150°C. Al-doped ZnO microrods also show a moderate response values towards acetone even at room temperature. The response and recovery time are found to be very fast of 110 ms and 960 ms of 3wt% Al-doped ZnO microrods for the detection of acetone vapor at room temperature, respectively. The results

indicate that Al-doped ZnO microrods sensor has a great potential for detecting ethanol and acetone vapor at low temperature.

Acknowledgments

Authors thankfully acknowledge the funding received from SERB (DST), New Delhi via grant no. EMR/2017/000058. SK also thankful to Royal Academy of Engineering Industry Academia program for funding. We thank Dr. Avishek Dey for XPS measurement.

References

[1] H.T. Nagle, S.S. Schiffman, The how and why of electronic noses, IEEE spectrum 35 (1998) 22–31.

[2] K.H. Kim, S.A. Jahan, E. Kabir, A review of breath analysis for diagnosis of human health, TrAC Trends Anal. Chem. 33 (2012) 1–8.

[3] A.K. Ruchika, Performance analysis of Zinc oxide based alcohol sensors, Int. J App. Sc. Engg. Res. 4 (2015) 427–436.

[4] T. Seiyama, A. Kato, K. Fujiishi, M. Nagatani, A new detector for gaseous components using semiconductive thin film, Anal. Chem. 34 (1962) 1502–1503.

[5] J. Guo, J. Zhang, M. Zhu, D. Ju, H. Xu, B. Cao, High performance gas sensor based on ZnO nanowires functionalized by Au nanoparticles, Sens. Actuat. B: Chem. 199 (2014) 339–345.

[6] J.J. Liu, M.H. Yu, W.L. Zhou, Well-aligned Mn-doped ZnO nanowires synthesized by a chemical vapor deposition method, Appl. Phys. Lett. 87 (2005) 172505–172508.

[7] L. Zhu, M. Zhi, Z. Ye, B. Zhao, Catalyst-free two-step growth of quasi-aligned ZnMgO nanorods and their properties, Appl. Phys. Lett. 88 (2006) 113106–113109.

[8] C. Xu, J. Chun, D. Kim, J.J. Kim, B. Chon, T. Joo, Elctrical properties and near band edge emission of Bi-doped ZnO nanowires, Appl. Phys. Lett. 90 (2007) 083113–083116.

[9] X. Qu, D. Jia, Controlled growth and optical properties of Al^{3+} doped ZnO nanodisks and nanorod clusters, Mater. Lett. 63 (2009) 412–414.

[10] F. Cao, C. Li, M. Li, H. Li, X. Huang, B. Yang, Direct growth of Al-doped ZnO ultrathin nanosheets on electrode for ethanol gas sensor application, Appl. Surf. Sci. 447 (2018) 173–181.

[11] S.C. Navale, V. Ravi, Low temperature synthesis and NO_x sensing properties of nanostructured Al-doped ZnO, Sens. Actuat. B: Chem. 126 (2007) 382–386.

[12] P.P. Sahay, R.K. Nath, Al-doped ZnO thin films as methanol sensors, Sens. Actuat. B: Chem. 134 (2008) 654–659.

[13] L.M. Li, Z.F. Du, T.H. Wang, Enhanecd sensing properties of defect controlled ZnO nanotetrapods arising from aluminium doping, Sens. Actuat. B: Chem. 147 (2010) 165–169.

[14] S.S. Badadhe, I.S. Mulla, Effect of aluminium doping on structural and gas sensing properties of zinc oxide thin films deposited by spray pyrolysis, Sens. Actuat. B: Chem. 156 (2011) 943–948.

[15] L. Vayssieres, K. Keis, S.E. Lindquist, A. Hagfeldt, Purpose-built anisotropic metal oxide material: 3D highly oriented microrod array of ZnO, J. Phys. Chem. B 105 (2001) 3350–3352.

[16] B.D. Yao, Y.F. Chan, N. Wang, Formation of ZnO nanostructures by a simple way of thermal evaporation, Appl. Phys. Lett. 81 (2002) 757–759.

[17] H. Yuan, Y. Zhang, Preparation of well-aligned ZnO whiskers on glass substrate by atmospheric MOCVD, J. Cryst. Growth 263 (2004) 119–124.

[18] Y.W. Heo, V. Varadarajan, M. Kaufman, K. Kim, D.P. Norton, F. Ren, P.H. Fleming, Site specific growth of ZnO nanorods using catalysis-driven molecular-beam epitaxy, Appl. Phys. Lett. 81 (2002) 3046–3048.

[19] L.E. Greene, M. Law, J. Goldberger, F. Kim, J.C. Johnson, Y. Zhang, R.J. Saykally, P. Yang, Low-temperature wafer-scale production of ZnO nanowire arrays, Angew. Chem., Int. Ed. 42 (2003) 3031–3034.

[20] J. Zhang, X. Liu, G. Neri, N. Pinna, Nanostructured materials for room- temperature gas sensors, Adv. Mater. 28 (2016) 795–831.

[21] O. Lupan, V. Postica, M. Hoppe, N. Wolff, O. Polonskyi, T. Pauporté, B. Viana, O. Majérus, L. Kienle, F. Faupel, R. Adelung, PdO/PdO_2 functionalized ZnO: Pd films for lower operating temperature H_2 gas sensing, Nanoscale 10 (2018) 14107–14127.

[22] R. Ghosh, M. Dutta, D. Basak, Self-seeded growth and ultraviolet photoresponse properties of ZnO nanowire arrays, Appl. Phys. Lett. 91 (2007) 073108-1–073108-3.

[23] T.T. Trinh, N.H. Tu, H.H.Le, K.Y. Ryu, K.B. Le, K. Pillai and J. Yi, Improving the ethanol sensing of ZnO nano-particle thin films-The correlation between the grain size and the sensing mechanism, Sens. Actuat. B: Chem. 152 (2011) 73–81.

[24] Y.E. Lee, Y.J. Kim, H.J. Kim, Thickness dependence of microstructural evolution of ZnO films deposited by rf magnetron sputtering, J. Mater. Res. 13 (1998) 1260–1265.

[25] H. Li, Z. Zhang, J. Huang, R. Liu, Q. Wang, Optical and structural analysis of rare earth and Li co-doped ZnO nanoparticles, J. Alloys Compd. 550 (2013) 526–530.

[26] Z. Yang, Q. Liu, H. C. Yu, B. Zou, Y.G. Wang, T. H. Wang, Substrate-free growth, characterization and growth mechanism of ZnO nanorod close-packed arrays, Nanotechnology 19 (2008) 035704–035709.

[27] R. C. Pawar, J. S. Shaikh, A. V. Moholkar, S. M. Pawar, J. H. Kim, J. Y. Patil, S. S. Suryavanshi, P. S. Patil, Surfactant assisted low temperature synthesis of nanocrystalline ZnO and its gas sensing properties, Sen. Actuat. B: Chem. 151 (2010) 212–218.

[28] M. Shaban, E.I. Sayed, Influences of lead and magnesium co-doping on the nanostructural, optical properties and wettability of spin coated zinc oxide films, Mater. Sci. Semicond. Process. 39 (2015) 136–147.

[29] S. Mridha, D. Basak, Aluminium doped ZnO films: electrical, optical and photoresponse studies, J. Appl. Phys. D 40 (2007) 6902–6907.

[30] R. S. Ganesh, G. K. Mani, R. Elayaraja, E. Durgadevi, M. Navaneethan, S. Ponnusamy, K. Tsuchiya, C. Muthamizhchelvan, Y. Hayakawa, ZnO hierarchical 3D-flower like architectures and their gas sensing properties at room temperature, Appl. Surf. Sci. 449 (2018) 314–321.

[31] S. Iaiche, A. Djelloul, $ZnO/ZnAl_2O_4$ Nanocomposite Films Studied by X-Ray Diffraction, FTIR, and X-Ray Photoelectron Spectroscopy, J. Spectroscopy 2015 (2015) 836859–9.

[32] A.A. Abokifa, K. Haddad, J. Fortner, C.S. Lo, P. Biswas, Sensing mechanism of ethanol and acetone at room temperature by SnO_2 nano-columns synthesized by aerosol routes: theoretical calculations compared to experimental results, J. Mater. Chem. A 6 (2018) 2063–2066

[33] S.C. Navale, V. Ravi, D. Srinivas, I.S. Mulla, S.W. Gosavi, S.K. Kulkarni, EPR and DRS evidence for NO_2 sensing in Al-doped ZnO, Sens. Actuat. B: Chem. 130 (2008) 668–673.

[34] G. Korotcenkov, Metal Oxides for Solid-state Gas Sensors: What Determines Our Choice? Mater. Sci. Eng. B 139 (2007) 1−23.

[35] S.Y. Lee, Sensing Properties of Ga-doped ZnO Nanowire Gas Sensor, Trans. Elect. Electron. Mater. 16 (2015) 78–81.

[36] Z. Yang, Y. Huang, G. Chen, Z. Guo, S. Cheng, S. Huang, Ethanol gas sensor based on Al-doped ZnO nanomaterial with many gas diffusing channels, Sens. Actuat. B: Chem. 140 (2009) 549–556.

[37] A.M. Sayed, S.M. Yakout, Highly sensing properties sensors based on Ce-doped ZnO and SnO_2 nanoparticles to ethanol gas, J. Res. Nanotech. 2016 (2016) 1–14.

[38] L. Zhang, J. Zhao, H. Lu, L. Gong, L. Li, J. Zheng, H. Li, Z. Zhu, High sensitive and selective formaldehyde sensors based on nanoparticle-assembled ZnO micro-octahedrons synthesized by homogeneous precipitation method, Sens. Actuat B: Chem. 158 (2011) 1440–1445.

[39] Y. Zhang, J. Xu, Brush-Like Hierarchical ZnO Nanostructures: Synthesis, Photoluminescence and Gas Sensor Properties, J. Phys. Chem. C 113 (2009) 3430–3435.

[40] M. Cargnello, V.V. Doan-Nguyen, T.R. Gordon, R.E. Diaz, E.A. Stach, R.J. Gorte, P. Fornasiero, C.B. Murray, Control of metal nanocrystal size reveals metal-support interface role for ceria catalysts, Science 341 (2013) 771–773.

[41] D. Zhang, A. Liu, H. Chang, B. Xia, Room-temperature high-performance acetone gas sensor based on hydrothermal synthesized SnO_2-reduced graphene oxide hybrid composite, RSC Adv. 5 (2015) 3016–3022.

[42] J.S. Do, S.H. Wang, On the sensitivity of conductimetric acetone gas sensor based on polypyrrole and polyaniline conducting polymers, Sens. Actuat B: Chem. 185 (2013) 39–46.

[43] B. Behera, S. Chandra, An innovative gas sensor incorporating ZnO-CuO nanoflakes in planar MEMS technology, Sens. Actuat. B: Chem. 229 (2016) 414–424.

[44] R. Yoo, S. Cho, M.J. Song, W. Lee, Highly sensitive gas sensor based on Al-doped ZnO nanoparticles for detection of dimethylmethylphosphonate as a chemical warfare agent stimulant, Sens. Actuat. B: Chem. 221 (2015) 217–223.

[45] L.A. Patil, A.R. Bari, M.D. Shinde, V. Deo, M.P. Kaushik, Detection of dimethyl methyl phosphonate – a simulant of sarin: the highly toxic chemical warfare –using platinum activated nanocrystalline ZnO thick films, Sens. Actuat. B: Chem. 161 (2012) 372–380.

[46] P. Zhang, G. Pan, B. Zhang, High Sensitivity Ethanol Gas Sensor Based on Sn-doped ZnO under visible light irradiation at low temperature, J. Mater. Res. 17 (2014) 817–822.

[47] M. Sinha, R. Mahapatra, B. Mondal, T. Maruyama, R. Ghosh, Ultrafast and reversible gas-sensing properties of ZnO nanowire arrays grown by hydrothermal technique, J. Phys. Chem. C 120 (2016) 3019–3025.

[48] T. Pauporte, O. Lupan, V. Postica, M. Hoppe, L. Chow, R. Adelung, Al-Doped ZnO Nanowires by Electrochemical Deposition for Selective VOC Nanosensor and Nanophotodetector, Phys. Status Solidi A 215 (2018) 1700824-1 –8.

[49] O. Lupan, L. Chow, T. Pauporte, L.K. Ono, B.R. Cuenya, G.Y. Chai, Highly sensitive and selective hydrogen single-nanowire nanosensor, Sens. Actuat. B: Chem. 173 (2012) 772–780.

[50] J. Guo, J. Zhang, M. Zhu, D. Ju, H. Xu, B. Cao, High-performance gas sensor based on ZnO nanowires functionalized by Au nanoparticles, Sen. Actuat. B: Chem. 199 (2014) 339–345.

[51] F. Hellegouarc'h, F. Arefi-Khonsari, R. Planade, J. Amouroux, PECVD prepared SnO_2 thin films for ethanol sensors, Sens. Actuators B 73 (2001) 27–34.

[52] A. Hazra, K. Dutta, B. Bhowmik, P. Bhattacharyya, Highly Repeatable Low-ppm Ethanol Sensing Characteristics of p-TiO_2-Based Resistive Devices, IEEE Sensors J. 15 (2015) 408–416.

[53] T. Samerjai, N. Tamaekong, C. Liewhiran, A. Wisitsoraat, A. Tuantranont, S. Phanichphant, Selectivity towards H_2 gas by flame-made Pt- loaded WO_3 sensing films, Sens. Actuat. B: Chem. 157 (2011) 290–297.

[54] A. Gurlo, Interplay between O_2 and SnO_2: Oxygen Ionosorption and Spectroscopic Evidence for Adsorbed Oxygen, Chem. Phys. Chem. 7 (2006) 2041–2052.

Figure Captions:

Fig. 1. (a) Schematic of the gas sensor structure, (b) original view of the sensor with the connections of two cupper probes, (c) top view of FE-SEM image of ZnO microds arrays.

Fig. 2. XRD patterns of undoped and Al-doped ZnO microrods along with standard JCPDS (card no.: 80-0075) of ZnO.

Fig. 3. AFM images of (a) 1wt%, (b) 2wt%, (c) 3wt% and (d) 4wt% Al-doped ZnO microrods.

Fig. 4. XPS spectra of undoped and 3wt% Al-doped ZnO microrods. High resolution XPS spectra of (a) Zn 2p, (b) O 1s, and (c) Al 2p.

Fig. 5. Response of different doping concentration of Al-doped ZnO microrods to 500 ppm of ethanol at an operating temperature of 150°C.

Fig. 6. Dynamic sensing characteristics toward ethanol at 150°C for 3wt% Al-doped ZnO microrods. Inset shows the typical response and recovery time toward 100 ppm ethanol sensing.

Fig. 7. Comparison of response as a function of concentration of ethanol and acetone at an operating temperature of 150°C for 3wt% Al-doped ZnO microrods.

Fig. 8. Dynamic sensing characteristics toward acetone vapor detecting at room temperature for 3wt% Al-doped ZnO microrods.

Fig. 9. Reliability study towards acetone detection at room temperature of 3wt% Al-doped ZnO microrods after 6 months.

Fig. 10. (a) Response-recovery curves for the sensor to 100 ppm acetone at room temperature, (b) Response time and (c) Recovery time of 3wt% Al-doped ZnO microrods sensor for all concentration.

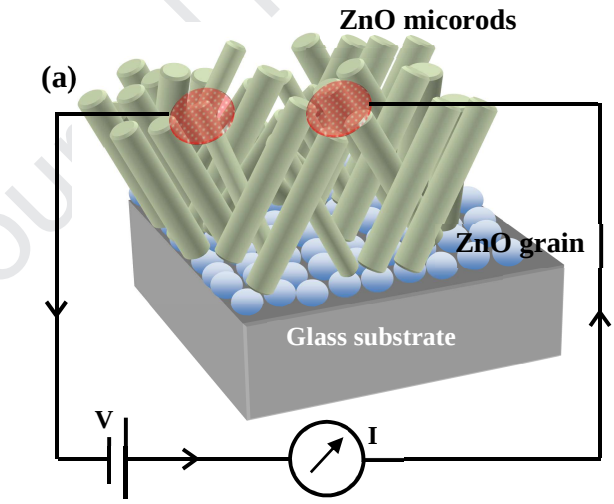

Figure 1

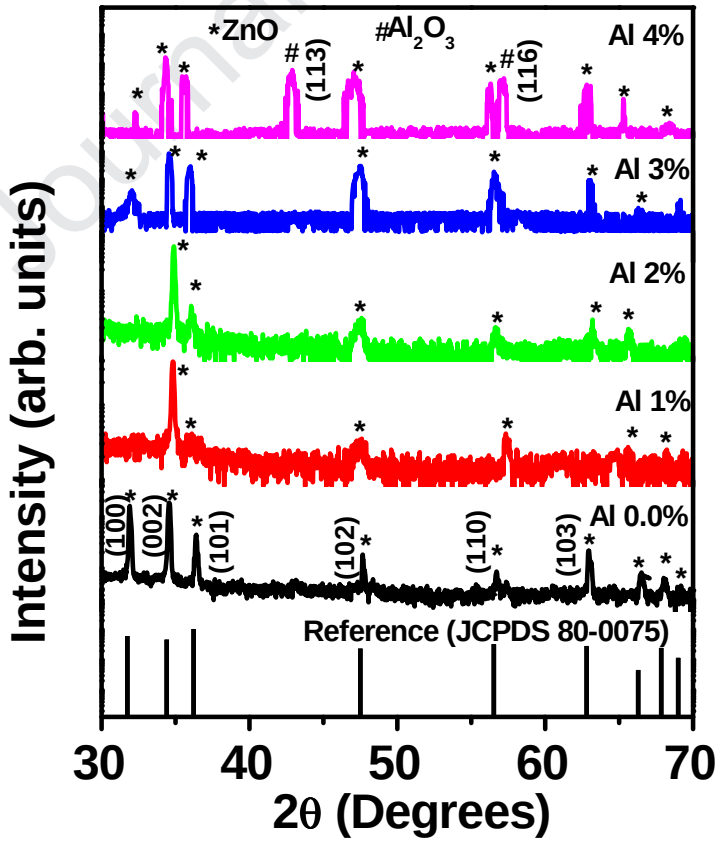

Figure 2

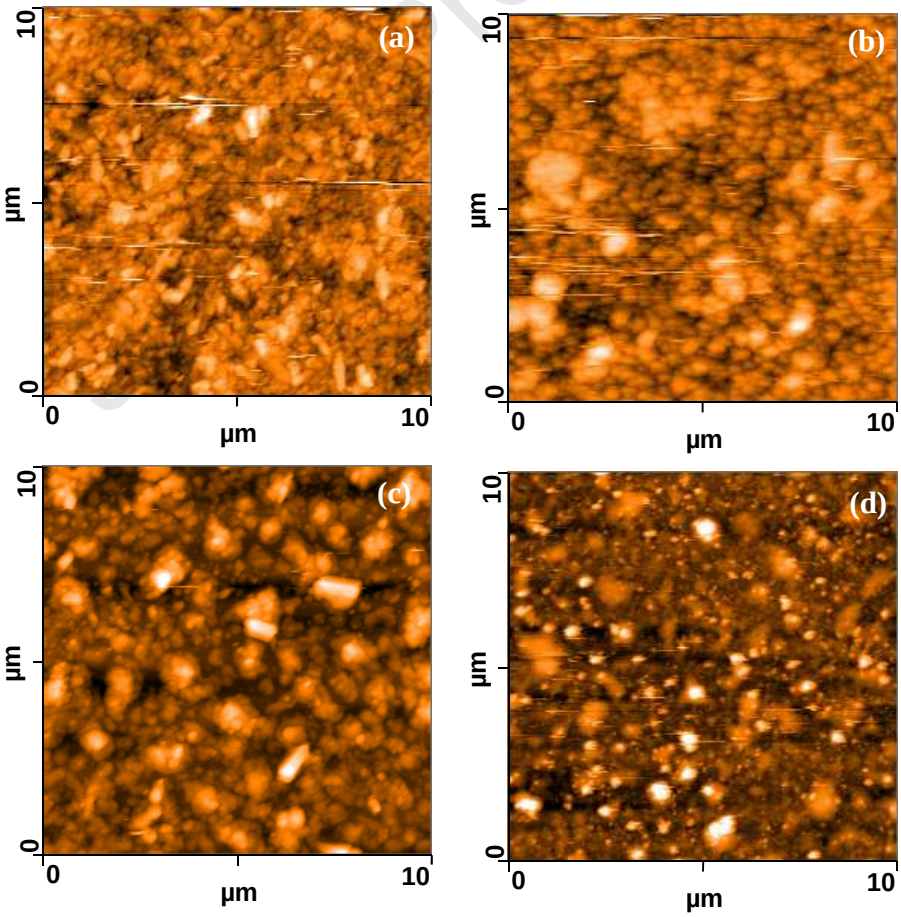

Figure 3

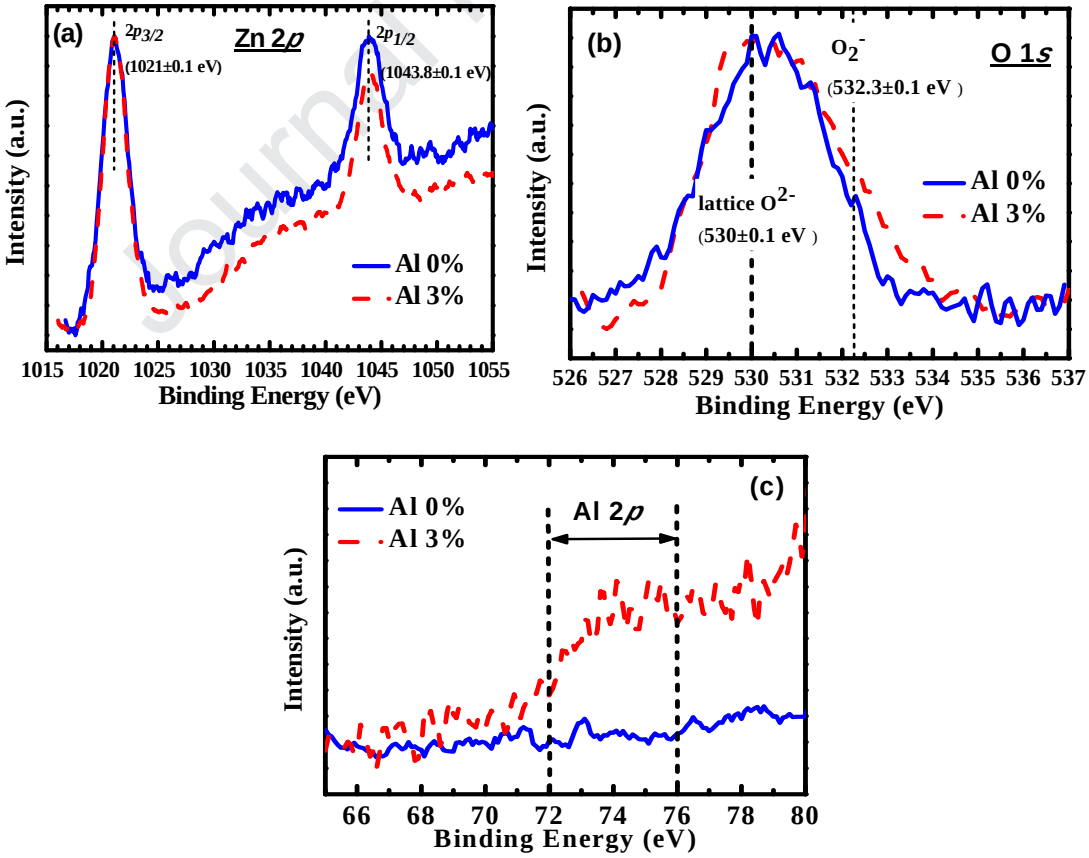
(a)
Zn 2p
2p3/2
(1021±0.1 eV)
2p1/2
(1043.8±0.1 eV)
Al 0%
Al 3%
Intensity (a.u.)
1015 1020 1025 1030 1035 1040 1045 1050 1055
Binding Energy (eV)
(b)
O 1s
O2-
(532.3±0.1 eV)
lattice O2-
(530±0.1 eV)
Al 0%
Al 3%
Intensity (a.u.)
526 527 528 529 530 531 532 533 534 535 536 537
Binding Energy (eV)
(c)
Al 0%
Al 3%
Al 2p
Intensity (a.u.)
66 68 70 72 74 76 78 80
Binding Energy (eV)

Figure 4

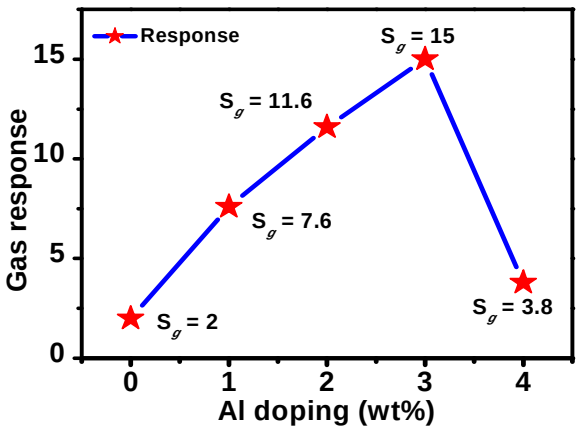

Figure 5

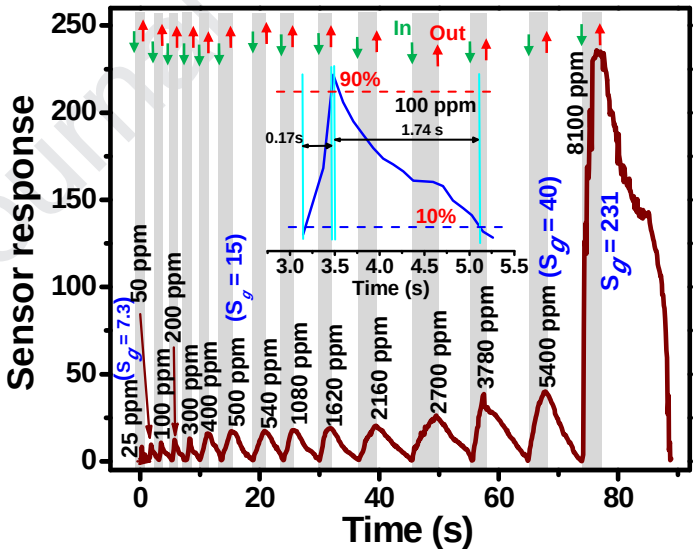

Figure 6

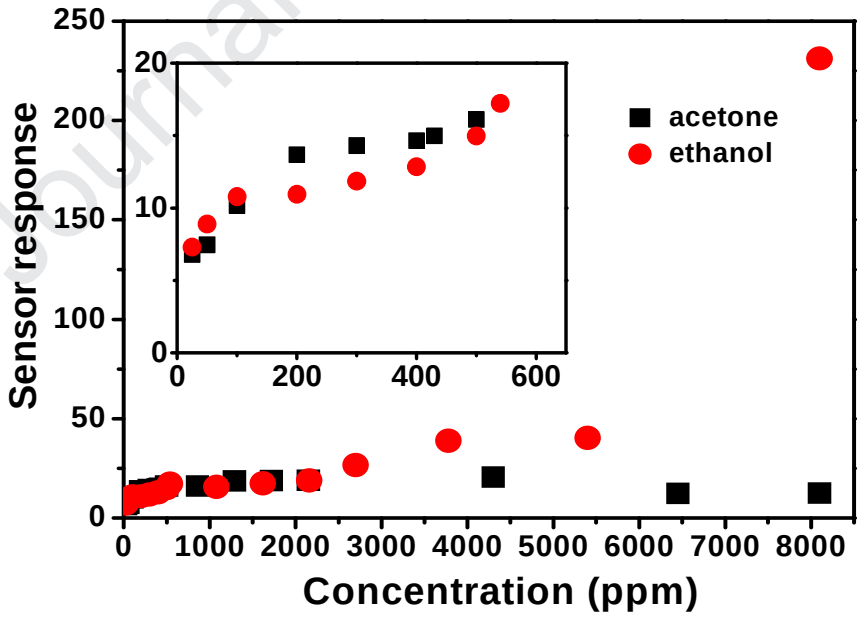

Figure 7

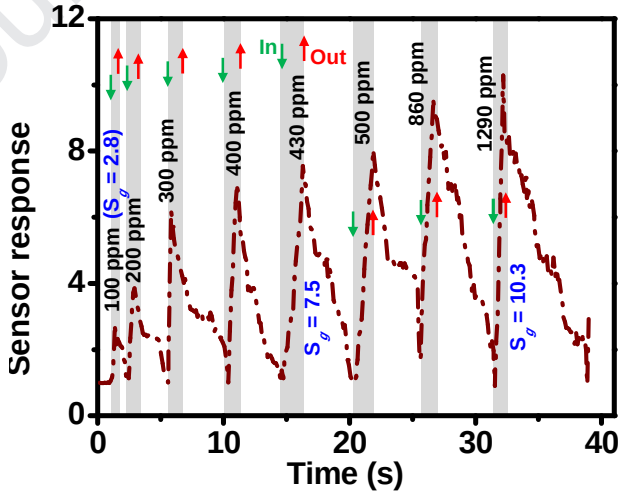

Figure 8

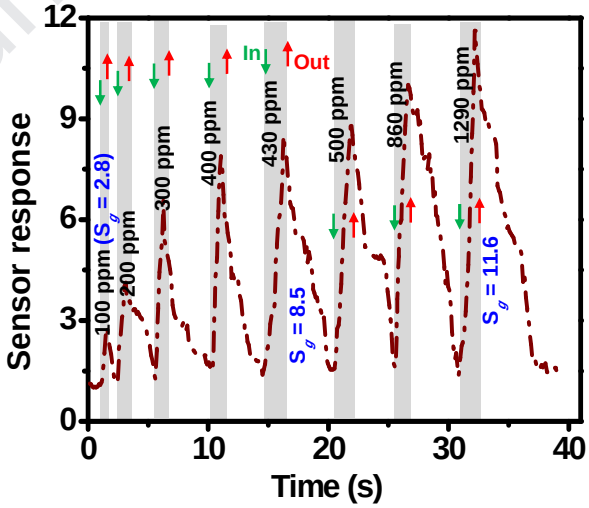

Figure 9

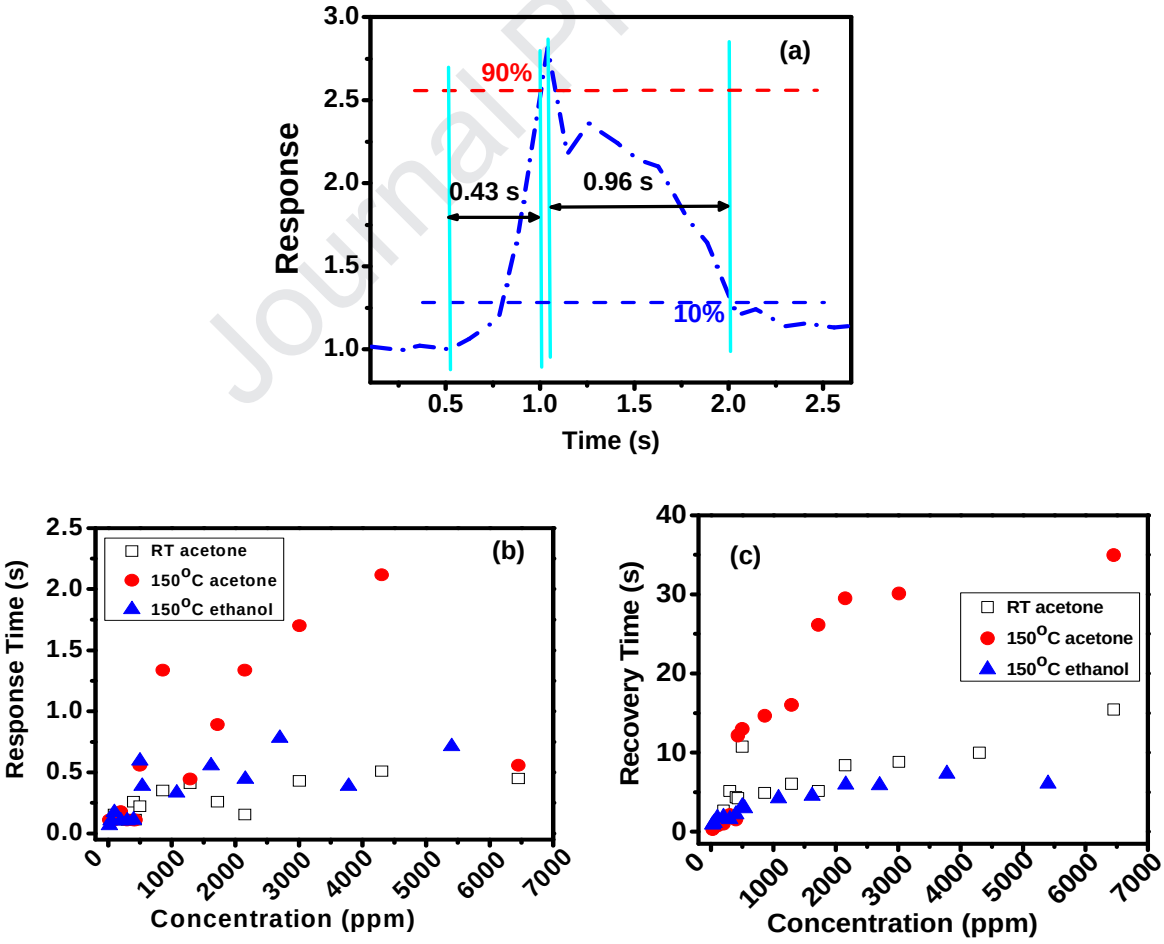

Figure 10

Table 1: Comparison between ethanol sensing properties of the different materials reports in pre-published and this work

Sample	**Concentration (ppm)**	**Temperature**	**Response**	**Response/ recovery time**	**Ref.**
Al-doped ZnO microrods	25-8100	150°C	7.3 – 231*	60 – 700 ms / 870 ms – 11.13 s	This work
Ga (3wt%) doped ZnO nanowire	1	300°C	48% [§]	-	35
Al (2 wt%) doped ZnO microstructure	3000	290°C	200[±]	8 s / 10 s	36
nanoparticles ZnO with 4 wt% CeO_2 and	100	400°C	85[¶]	12 s / 10 s	37
SnO_2 with 2 wt% CeO_2			120	20 s / 15 s	
Sn (5at.%, 7 at.%, 9 at.%) doped ZnO	1000	65°C	100[¶]	1 s / 5 s	46

*Response, $S_g = G_g/G_a$, [§]S_g (%) = $(R_g - R_a)/R_a \times 100$, [±]$S_g = R_{vapor}/R_{air}$, [¶]$S_g = R_{air}/R_{gas}$

Table 2: Comparison of gas sensing parameters of some gas sensor toward acetone

Sample	**Concentration (ppm)**	**Temperature**	**Response**	**Response time/ recovery time**	**Ref.**
Al:ZnO microrods	100 – 6450	RT	2.8–11.6[*]	110 – 510 ms / 960 ms – 15.4 s	This work
Al:ZnO microrods	25 – 6450	150°C	0.07 – 12.3[*]	110 ms–2.11 s / 330 ms–34.9 s	This work
SnO_2-RGO	10 – 2000	RT	2.19 – 9.72%[§]	107–146 s / 95–141 s	41
PPy-PANI	2983 – 47,925	RT	Sensitivity : 1.19 – 4.03×10^{-7} [±]	1.0–3.0 min / 3.0–10.0 min	42
ZnO–CuO nanoflakes	10	300°C	12.6[¶]	22 s / 26 s	43
Al doped (1wt%) ZnO nanoparticle	10 dimethylphosphonate	350°C	4347[¶]	2s	44

[*]Response, $S_g = G_g/G_a$, [§]S_g (%) = $(R_a - R_g)/R_g \times 100$, [±]$S_g = (R_g - R_a)/R_a$, [¶]$S_g = R_a/R_g$

RESEARCH HIGHLIGHTS:

- Al-doped ZnO microrods were synthesized by low-temperature hydrothermal technique.
- Room temperature acetone sensing is observed for Al-doped ZnO microrods.
- 3 wt% Al-doped ZnO microrods shows ultrafast detection (110 ms) towards acetone.

AUTHOR DECLARATION

We wish to draw the attention of the Editor to the following facts which may be considered as potential conflicts of interest and to significant financial contributions to this work. [OR]

We wish to confirm that there are no known conflicts of interest associated with this publication and there has been no significant financial support for this work that could have influenced its outcome.

We confirm that the manuscript has been read and approved by all named authors and that there are no other persons who satisfied the criteria for authorship but are not listed. We further confirm that the order of authors listed in the manuscript has been approved by all of us.

We confirm that we have given due consideration to the protection of intellectual property associated with this work and that there are no impediments to publication, including the timing of publication, with respect to intellectual property. In so doing we confirm that we have followed the regulations of our institutions concerning intellectual property.

We understand that the Corresponding Author is the sole contact for the Editorial process (including Editorial Manager and direct communications with the office). He/she is responsible for communicating with the other authors about progress, submissions of revisions and final approval of proofs. We confirm that we have provided a current, correct email address which is accessible by the Corresponding Author and which has been configured to accept email from ghosh.ranajit@gmail.com

Signed by all authors as follows:

1. Madhumita Sinha:

2. Rajat Mahapatra:

3. Manas Kumar Mondal:

4. Satheesh Krishnamurthy:

5. Ranajit Ghosh: